

## Improving the Small Signal Stability of a PV-DE-Dynamic Load-Based Micro grid using an Auxiliary Signal in the PV Control loop



**Parvatham Jayanthi**

**M.Tech,**

Arjun College of Technology and Sciences.



**T.Rakesh, M.Tech**

**Assistant Professor,**

Arjun College of Technology and Sciences.

### Abstract:

In this paper, a small signal model has been developed for a grid connected photovoltaic (PV)-diesel engine (DE) system feeding also to an induction motor at the low voltage level. The comprehensive mathematical model of the system has been developed by linearizing the system of equations around an operating point. To analyze the stability of the system, the eigen values and thus the modes of the system have been obtained from the result and analytical A matrix. Further, to validate this small signal model, a complete nonlinear time-domain analysis of the system has been carried out. In order to enhance the stability of the system, a supplementary controller in the PV control loop has been proposed and its results have been verified both from the eigen values and from the nonlinear analysis.

### Index Terms:

Distributed generation, induction motors, micro grids, photovoltaic stability.

### NOMENCLATURE:

The following notation has been used throughout this paper.

### Acronyms

- PV Photovoltaic.
- VSC Voltage source converter.
- DE Diesel engine.
- IPP Independent power producer.

- PCC Point of common coupling.
- AVR Automatic voltage regulator.

### PV Array

- $N_s$  Number of PV cells in series.
- $N_p$  Number of strings in parallel.
- $I_p, h, I_g$  Photocurrent and dark current.
- $q, T_c$  Charge of an electron and cell temperature.
- $K, A$  Boltzmann's constant and ideal factor.
- $P_{pv}, P_{dc}, P_t$  PV Array power, dc power into VSC and ac power from VSC.
- $C_{dc}, V_{dc}$  dc link capacitor and voltage.
- $X_{cs}, X_{fs}$  Filter and connecting line reactance.
- $i_d, i_q$  dq frame current components of VSC.
- $v_d, v_q$  dq frame voltage components of PCC.
- $m_d, m_q$  dq frame components of modulation index of VSC
- $V_{acb}, V_{dcb}$  ac and dc side voltage base.
- $\rho_1, \rho_2, K_g$  sliding mode controller gains.

### Diesel Engine

- $P_e$  ac power from DE.
- $X_t, H$  Winding reactance and inertia constant of DE
- $V_t, V_{ref}$  Terminal voltage and reference
- $w, \delta$  Angular velocity and torque angle.

- $P_m, E'_{fd}$  Input mechanical power, internal voltage and stator side exciter voltage.
- $K_{avr}, T_a$  AVR gain and time constant.
- $K_1, K_2, K_3$  Governor Gains.
- $T_1, T_2$  Governor time constants.
- $k_1, k_2$  Padé approximation constants.
- $i_{sd}, i_{sq}$  dq axis components of current.
- $X_d, X'_d, T'_d$  Direct axis steady state reactance, transient reactance and open circuit time constant.

### Induction Motor

- $J, T_e, T_m$  Inertia, electrical torque and mechanical torque.
- $\omega_r, s$  Induction motor angular velocity and slip.
- $R_r, X_r, X_m$  Induction motor resistance and inductance.
- $i_{ds}, i_{qs}$  axis components of current.
- $v'_d, v'_{qd}$  axis components of internal voltage.

### Network

- $R_{sb}, X_{sb}$  Resistance and reactance of line to main grid.
- $X_{sb2}$  Transformer reactance.
- $V_b$  Infinite bus voltage magnitude.

## I. INTRODUCTION:

As fossil fuel reserves deplete and environmental concerns increase, the need for clean and plentiful methods of energy production has brought about an increased presence of photovoltaic and wind energy systems. Efficient extraction of energy from these clean sources is vital to meeting the demands of the ever growing electricity grid. Being in a nascent state, these sources are often coupled with diesel generators and a combination of such sources is used to serve small regions of the system. As with any controllable distributed generation source, the effect of these sources on the small signal stability of the system has to be analyzed.

Both wind and solar energy systems require a grid side interfacing voltage source converter (VSC) due to the asynchronous operation of the wind turbine and the dc output of a solar array. As has been discussed in [1], if the VSC is not controlled in a proper manner, it can lead to instability in the system. A general approach towards evaluating stability in converter interfaced microgrids has been discussed in [2]–[6]. With conventional synchronous machines, the inherent property of the machine gives rise to the concept of synchronizing torque which is instrumental in providing first swing stability. Further, the combination of the machine inertia and the requirement for locking of the poles of the rotor and stator magnetic field gives rise to a damping torque when a disturbance occurs. However, with converter interfaced generation like wind and solar these inherent torques are very low, if not altogether absent. In [7], the authors have developed a small signal model for a microgrid containing a fuel cell as the distributed generation source. However, the penetration of fuel cells in the distribution network is marginal when compared to the penetration of PV arrays and wind generators.

The small signal analysis of microgrids with wind generators has been well documented in literature [8]–[12]. With solar however, the literature is not as well established. [13] Develops the small signal model of an isolated PV array delivering a load while [14]–[16] have analyzed the small signal stability of large scale PV generation at the transmission level. Although the analysis at the transmission level is of vital importance in order to assess the stability of inter connected systems, it requires utility level installation of solar parks. With the micro-grid lobby gaining momentum and with government incentives for installation of renewable energy, small scale “rooftop” PV sources are very much a reality in the near future. The published literature is found lacking in the analysis of the stability of distribution system connected sources. A majority of the analysis is with regard to the effects of the PV sources on the voltage regulation of the distribution system as has been seen in [17] and [18]

and mentioned in [15]. In [19], an analysis of a PV-diesel generator system connected to an infinite bus via a transmission line is presented. The results show that as the contribution of the PV source increases, the damping ratio progressively decreases and after a certain point the system becomes unstable. These results have a close connection with the results presented in [7]. In both, the VSC of the alternate energy source is controlled by using linear controllers. Using a similar system configuration, a small signal model for a PV-diesel generator microgrid has been developed in [20]. However in [20], the VSC is controlled using a nonlinear sliding mode controller developed on the lines of [21] and [22]. Using this nonlinear controller it has been shown that the system remains stable at all levels of contribution from the PV source.

One of key points that have been overlooked by the present literature is the effect of load behavior, in particular induction motor loads, on the transient stability of PV systems that are interfaced at the distribution level. The general impact of such loads on the stability of the transmission network has been well analyzed. Due to the high R/X ratio in distribution systems [23], it is assumed that these motor loads would not affect the stability of the system. In addition, in [15], the system has been analyzed considering the presence of both rooftop PV and utility installed PV sources with the rooftop PV sources modeled as constant negative loads, the assumption being that these sources would not have a say in the stability of the larger system.

In this paper, it will be shown that with an ever increasing percentage of microgrids across the system, this assumption will not hold water. A section of a distribution system is considered modeled on the lines of the system in [20]. In addition, an induction motor load is considered to be connected on the low voltage side of the system and the diesel generator is assumed to be fitted with a governor. With the inclusion of the dynamic load, it is shown that the stability margin of the system drastically reduces.

It has also been proposed to add an auxiliary signal to the control loop of the VSC of the PV array in

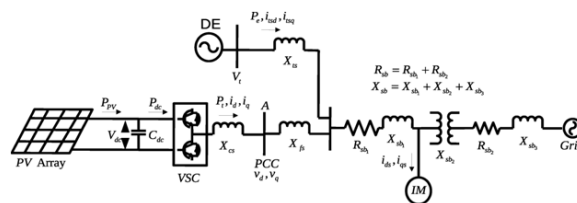


**Fig. 1. Single line diagram of PV-diesel generator system.**

order to stabilize the system. This option is more economical when compared to system stabilization using energy storage elements or demand side response wherein incentives will have to be provided to consumers. On the basis of the small signal model developed in [24] for the induction motor and the transfer function model in [25] for the governor, a complete model for the small signal analysis of this system has been developed. The paper is organized as follows. The system considered is described in Section II with the development of the mathematical model described in Section III. Section IV describes the results obtained from the analysis while Section V concludes the paper.

## II. SYSTEM MODEL

The system considered is as shown in Fig. 1. The sources of power in the microgrid are the PV array and the DE. The PV array is interfaced by means of a VSC which is in charge of providing only active power support. This is in line with the grid code which restricts inverter interfaced sources from controlling the voltage at a bus. The voltage control is performed by the DE which is equipped with an automatic voltage regulator (AVR). In addition, to ensure completeness of the model, the DE also has a governor. The power extracted from the PV array is governed by (1). For a given solar isolation level and cell temperature, the PV array power  $P_{pv}$  and the dc voltage  $V_{dc}$  across the capacitor  $C_{dc}$  are related as shown by characteristics in Fig. 2.

$$P_{pv} = \left( N_p I_{ph} - N_p I_s \left[ \exp \left( \frac{qV_{dc}}{N_s k T C_A} \right) - 1 \right] \right) V_{dc} \quad (1)$$

Thus by changing the voltage across the capacitor, the power extracted from the PV array can be varied. In this manner, different ratios of power sharing can be achieved between the DE and the PV array. An induction motor load is assumed to be connected to the system at a point before the connection to the main grid.

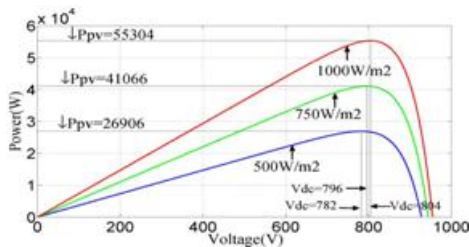


**Fig. 2. Power versus dc link voltage for the PV array.**

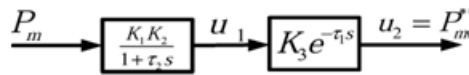


**Fig. 3. DE governor block diagram.**

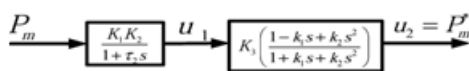


**Fig. 4. DE governor block diagram with Padé approximation.**

**MATHEMATICAL MODEL**

The dynamics of the system depicted in Fig. 1 is governed by multiple differential equations as described below:

**GOVERNOR:**

The governor, as shown in Fig. 3, is represented by a dead time constant  $T_1$  and an actuator time constant  $T_2$ . The dead time is a feature of depicting the amount of time it takes for the fuel change command to be reflected as a change in the output power of the DE [25].

The gains  $K_1$  and  $K_2$  represent the actuator constant and the current driver constant respectively while the engine torque constant is represented by  $K_3$ . As the dead time is an irrational function, it is approximated as a rational function using the Padé approximation. A second order approximation is sufficient for the study carried out as the phase response of the Padé approximation closely matches the phase response of the actual dead time for the interested range of frequencies. The block diagram of the governor with the Padé approximation is shown in Fig. 4 where  $K_1 = T_1/2$  and  $K_2 = T_1^2/12$ . As a result, the equations of the governor is as follows:

$$\frac{du_1}{dt} = \left( \frac{-1}{T_2} \right) u_1 + \left( \frac{K_1 K_2}{T_2} \right) P_m \quad (2)$$

$$\frac{du_2}{dt} = u_3 \quad (3)$$

$$\begin{aligned} \frac{du_3}{dt} = & \left( \frac{K_3}{k_2} + \frac{K_3 K_1}{T_2 k_2} + \frac{K_3}{T_2^2} \right) u_1 - \frac{u_2}{k_2} - \frac{k_1}{k_2} u_3 \\ & - \left( \frac{k_1 K_1 K_2 K_3}{T_2 k_2} + \frac{K_1 K_2 K_3}{T_2^2} \right) P_m \end{aligned} \quad (4)$$

Due to the second order Padé approximation, a need arises for a fictitious state variable to characterize the dynamics of the dead time block. Thus  $u_2$  and  $u_3$  are the state variables that represent the dynamics of the dead time block with  $u_3$  being the fictitious state variable as can be seen from (3).

**DIESEL GENERATOR**

The synchronous generator of the diesel generator has been modeled using the well known single axis simplified model. In addition, the exciter has been modeled as a simple first order time constant [26].

**PV ARRAY:**

$$\frac{dV_{dc}}{dt} = \frac{w}{C_{dc}} \left( \frac{V_{acb}}{V_{dcb}} \right)^2 \left( \frac{P_{pv}}{V_{dc}} - \frac{v_d i_d}{V_{dc}} - \frac{v_q i_q}{V_{dc}} \right) \quad (5)$$

$$\frac{di_d}{dt} = w i_q - \frac{w v_d}{L_f} + \frac{m_d w V_{dc} V_{dcb}}{L_f V_{acb}} \quad (6)$$

$$\frac{di_d}{dt} = -w i_q - \frac{w v_d}{L_f} + \frac{m_d w V_{dc} V_{dcb}}{L_f V_{acb}} \quad (7)$$

Where  $L_f$  is the inductance corresponding to the filter reactance and its value is equal to  $X_{cs}$  in per unit. In these equations, the values of the dc capacitance  $C_{dc}$  and the filter inductance  $L_f$  are taken in per unit. As a result,  $w$  appears in the equations as

$$L_{base} = Z_{base}/w \quad C_{base} = Y_{base}/w$$

The VSC of the PV array is controlled using a second order sliding mode controller as discussed in [21]. Due to formation of the second order system, an additional state variable is formed for the PV system. The equation for this additional state variable is derived from (5)–(7) and is as represented in (8):

$$\begin{aligned} \frac{dV_{dc}}{dt} &= g \\ \frac{dg}{dt} &= \frac{\lambda_1' w V_{acb}^2}{C_{dc} C_{dcb}^2} + \frac{-m_d w^2 V_{acb} v_d}{L_f C_{dc} V_{dcb}} \\ &\quad + \frac{-m_q w^2 V_{acb}}{L_f C_{dc} V_{dcb}} \end{aligned} \quad (8)$$

Where

$$\lambda_1' = -\frac{g \lambda_2'}{V_{dc}} - \frac{w i_q v_d}{V_{dc}} + \frac{w v_d^2}{V_{dc} L_f} + \frac{w i_d v_q}{V_{dc}} + \frac{w v_q^2}{V_{dc}}$$

$$\lambda_2' = -\frac{P_{pv}}{V_{dc}} - \frac{v_d i_d}{V_{dc}} - \frac{v_q i_q}{V_{dc}}$$

The concept of the sliding mode controller is to define a sliding surface for the variables of interest and the control philosophy operates in such a manner so as to bring the said variables onto this surface. The usual surfaces that are defined are for the error between the reference value of a variable and its actual value. In controlling the VSC of the PV array, the differential variables  $V_{dc}$  and  $i_q$  are the variables of interest. Thus a sliding surface is defined for each of these variables. The expressions for the control,  $m_d$  and  $m_q$  are obtained as given in (9) and (10):

$$m_q = \frac{\left( -\rho_2 \tanh(i_q - i_{qref}) + \omega i_d + \frac{\omega v_q}{L_f} \right) L_f V_{acb}}{\omega V_{dc} V_{dcb}} \quad (9)$$

$$m_d = \frac{\left( -\left( \rho_1 \tanh(g + k(V_{dc} - V_{dcref})) + kg \right) - \frac{\lambda_1' \omega V_{acb}^2}{C_{dc} V_{dcb}^2} + \frac{\omega^2 V_{acb} v_q m_q}{L_f C_{dc} V_{dcb}} \right) L_f C_{dc} V_{dcb}}{-\omega^2 V_{acb} v_d} \quad (10)$$

**INDUCTION MOTOR:**

The induction motor has been represented as a three equation model as described in [27] with one swing equation and two voltage differential equations.

The entire state variable set can be represented as  $x = [u_1 \ u_2 \ u_3 \ \delta \ w_{de} \ E_q' \ E_{fd} \ V_{dc} \ i_d \ i_q \ w_{rind} \ v_d' \ v_q']^T$

In order to obtain the state space model of the system, the algebraic equations have to be represented in terms of the differential variables. The independent algebraic variables are  $i_{ds}$ ,  $i_{qs}$ ,  $i_{tsq}$ ,  $i_{tsd}$ ,  $v_d$  and  $v_q$ . All other algebraic variables can be represented in terms of these variables. The current operating point for the system is obtained by running a power flow. To incorporate the initialization of the induction motor parameters, the procedure as detailed in [28] has been incorporated into the Newton Raphson algorithm. With the operating point so obtained, the linearization of the equations is carried out to obtain the system state matrix. Thus, the state matrix obtained is as given in (14), shown at the bottom of the next page. The expressions for these elements are specified in the Appendix.

The small signal stability of the system is analyzed by obtaining the eigen values of the above constructed state matrix.

### III. SIMULATION AND RESULTS:

The roots of the state matrix in (14) are the eigen values of the system. Table I shows the variation in the oscillatory modes along with the participating states and contributing element with change in the power generation ratio. The induction motor load is assumed to be 0.2 pu while the PV array is operated in a constant power mode by derating it. It can be seen that there are three oscillatory modes present in the system. The first oscillatory mode, represented by  $\lambda_1$  is predominantly due to the electrical transients in the induction motor. The damping ratio of the mode can be calculated from the eigen value  $\lambda = \sigma \pm j\omega$  as given by (11) [27]:

$$\delta = \frac{-\sigma}{\sqrt{\sigma^2 + \omega^2}} \quad (11)$$

Thus, the damping ratio for this mode is  $\delta = 0.91$ . This mode is hence highly damped and is of not much concern. The second oscillatory mode, represented by  $\lambda_2$  is the electromechanical mode of oscillation due to the DE. This mode is of prime importance as it causes the system to become unstable due to its relatively low damping ratio which varies from  $\delta = 0.002$  at  $P_{pv}=0.1$ pu and  $P_{de}=0.1$ pu to  $\delta = -0.007$  at  $P_{pv}=0.9$ pu and  $P_{de}=0.1$ pu. The third oscillatory mode, represented by  $\lambda_3$  is due to the governor of the DE. An oscillatory mode occurs due to the modelling detail of the Padé approximation. As a second order approximation has been used, an oscillatory mode arises. The second order approximation is the minimum level of approximation required because the phase response matches the phase response of the actual irrational function in the frequency range of interest. However, again, this mode is highly damped with a damping ratio of  $\delta = 0.866$  and is thus of little concern. As the penetration of the PV power increases, with the presence of dynamic local load it can be seen that the system becomes unstable at 0.3 pu.

This is in contrast to the earlier results that have been obtained in [20] wherein the system was stable at all power levels without the presence of the induction motor load. The reason for the change in the stability of the system is the presence of the induction motor. This can be concluded by comparing the electromechanical modes in both cases. Table II shows the variation in the electromechanical mode as the penetration of PV power increases in the system both with and without the induction motor load.

TABLE I: OSCILLATORY MODES FROM ANALYTICAL STATE MATRIX

$P_{pv}$ (pu)	$P_{de}$ (pu)	$\lambda_1$	$\lambda_2$	$\lambda_3$
0.1	0.9	-61.467 $\pm 27.93j$	-0.021 $\pm 10.182j$	-12 $\pm 6.928j$
0.2	0.8	-61.464 $\pm 27.927j$	-0.005 $\pm 10.113j$	-12 $\pm 6.928j$
0.3	0.7	-61.462 $\pm 27.924j$	0.01 $\pm 10.093j$	-12 $\pm 6.928j$
0.4	0.6	-61.462 $\pm 27.922j$	0.025 $\pm 10.076j$	-12 $\pm 6.928j$
0.5	0.5	-61.464 $\pm 27.922j$	0.039 $\pm 10.082j$	-12 $\pm 6.928j$
0.6	0.4	-61.47 $\pm 27.925j$	0.052 $\pm 10.114j$	-12 $\pm 6.928j$
0.7	0.3	-61.479 $\pm 27.93j$	0.063 $\pm 10.176j$	-12 $\pm 6.928j$
0.8	0.2	-61.492 $\pm 27.938j$	0.072 $\pm 10.282j$	-12 $\pm 6.928j$
0.9	0.1	-61.512 $\pm 27.954j$	0.075 $\pm 10.491j$	-12 $\pm 6.928j$
Participating States		$\omega_{r,ref} = 13\%$ $v_d^* = 45\%$ $v_q^* = 42\%$	$\delta = 48\%$ $\omega_{de} = 48\%$	$u_2 = 50\%$ $u_3 = 50\%$
Contributing Element		Induction Motor	Synchronous Generator	Governor Dead Time

TABLE II: ELECTROMECHANICAL MODE

Ratio	Electromechanical Mode(With IM)	Electromechanical Mode(Without IM) [20]
PV=0.1 DE=0.9	-0.02089 $\pm 10.18221j$	-0.02275 $\pm 9.943224j$
PV=0.2 DE=0.8	-0.005471 $\pm 10.12956j$	-0.085297 $\pm 9.884158j$
PV=0.3 DE=0.7	0.010087 $\pm 10.093122j$	-0.068366 $\pm 9.841058j$
PV=0.4 DE=0.6	0.025203 $\pm 10.076238j$	-0.052251 $\pm 9.817643j$
PV=0.5 DE=0.5	0.039328 $\pm 10.081889j$	-0.037699 $\pm 9.817328j$
PV=0.6 DE=0.4	0.052095 $\pm 10.113733j$	-0.025361 $\pm 9.841803j$
PV=0.7 DE=0.3	0.062959 $\pm 10.176314j$	-0.015904 $\pm 9.902166j$
PV=0.8 DE=0.2	0.071552 $\pm 10.281989j$	-0.009974 $\pm 10.003444j$
PV=0.9 DE=0.1	0.075339 $\pm 10.490948j$	-0.019451 $\pm 10.204166j$

In both cases, as the proportion of DE power decreases the damping ratio of the electromechanical mode becomes less positive. This, at first, appears to be somewhat erroneous as when the DE power decreases its torque angle reduces and thus the amount of synchronizing torque increases.

However, the amount of damping torque that is present in the system decreases as the synchronizing torque increases. This can be explained by considering a single machine infinite bus model as in [27]. With  $K_s$  representing the synchronizing torque coefficient, the equation for the damping ratio can be written as

$$\delta = \frac{1}{2} \frac{D}{\sqrt{K_s^2 H w_0}} \quad (12)$$

It can be seen that as the synchronizing torque increases the damping ratio decreases. Since the PV array is operated in a constant power mode, the PV-DE system can be considered as a single machine connected to the infinite bus. Thus as the pro-portion of DE power decreases, the damping ratio also becomes less positive as has been explained above

**TABLE III: OSCILLATORY MODES AFTER ADDITION OF AUXILIARY SIGNAL**

$P_{pv}$ (pu)	$P_{de}$ (pu)	$\lambda_1$	$\lambda_2$	$\lambda_3$
0.1	0.9	-61.975 ± 27.046j	-0.092 ± 10.317j	-12 ± 6.928j
0.2	0.8	-62.001 ± 26.926j	-0.078 ± 10.293j	-12 ± 6.928j
0.3	0.7	-62.043 ± 26.758j	-0.063 ± 10.298j	-12 ± 6.928j
0.4	0.6	-62.11 ± 26.513j	-0.05 ± 10.341j	-12 ± 6.928j
0.5	0.5	-62.217 ± 26.136j	-0.038 ± 10.44j	-12 ± 6.928j
0.6	0.4	-62.403 ± 25.49j	-0.028 ± 10.627j	-12 ± 6.928j
0.7	0.3	-62.771 ± 24.194j	-0.023 ± 10.984j	-12 ± 6.928j
0.8	0.2	-63.806 ± 20.286j	-0.023 ± 11.834j	-12 ± 6.928j
0.9	0.1	-104.453 ± 8.196j	0.268 ± 16.894j	-12 ± 6.928j

Using the concept behind a power system stabilizer (PSS), an auxiliary signal proportional to the frequency deviation can be used to change the PV power levels to operate the PV array in a variable power mode in order to stabilize the system.

Thus, the dc voltage reference of the PV array can now be given as in (13):

$$V_{dcref} = V_{dcref0} + k_1 \Delta w \quad (13)$$

The effect of the auxiliary signal can be seen from the plots. The frequency of oscillation both without and with the auxiliary signal remains the same as can be seen from the eigen values in Tables I and III and from the inset in Fig. 5(a) and (b). From the inset it can be seen that the time period of the oscillation is 0.61 s. Thus the frequency of the oscillation is 1.64 Hz or 10.3 rad/s. The slight difference in the frequency between the eigen value and the time-domain simulation can be accounted for due to the approximation in linearizing the system. There is however, a significant increase in the damping of the oscillatory electromechanical mode. The change in the PV power due to the change in dc voltage reference can be observed from Fig. 8. It can be seen that there is very little change in the PV power from the steady state value. Thus with the introduction of a little change in the input PV power, the system stability can be improved.

**V. CONCLUSION:**

In this paper, a small signal model for a PV-DE microgrid with a dynamic load has been developed. The eigen value analysis of the system has been carried out to show the change in stability with the increased penetration of the PV source. Under such circumstances, while analyzing large systems, it cannot be assumed that the small microgrids will not have an effect on the stability of the overall system. An unstable microgrid can cause a cascading effect on the entire system thereby driving the en-tire system to instability. In addition, a comparison between the stability of the system both with and without an induction motor load has been shown to illustrate the effect of the induction motor on the system stability. An auxiliary control signal has been proposed to stabilize the system. The effect of this auxiliary signal has been validated from both the eigen values and a full blown nonlinear time-do-main simulation of the system.

With the addition of the auxiliary signal, the PV array contributes some amount of damping torque to the system. The magnitude and sign of this torque is proportional to the value assumed for the variable  $k_1$  in (17). Evaluation of this torque and its sensitivity to the value  $k$  is an area of future research. The model can also be used in situations with conventional synchronous machines. The oscillatory mode produced by the state variables  $u_2$  and  $u_3$  are as a result of the dead time in the diesel generator.

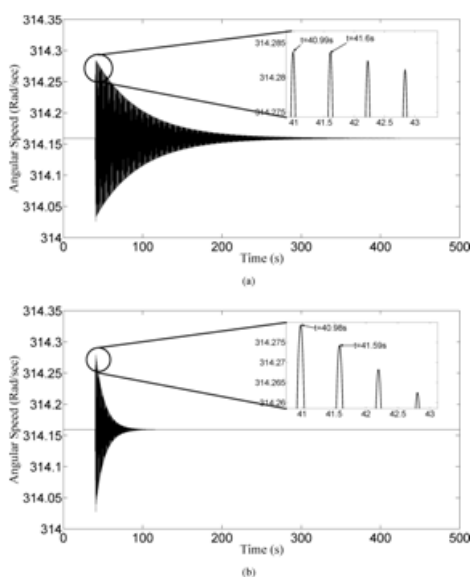


**Fig. 5. DE speed for  $PV=01$  pu. (a) Without auxiliary signal. (b) With auxiliary signal Governor.**

This mode will thus not exist with conventional synchronous machines and governors. This model, being a complete one, can be used for the analysis of the stability of large integrated systems. By using model reduction techniques as developed in [29] and by considering an aggregation of induction motors in the distribution system [30], a reduced model of this system can be developed and this reduced model can be used in the analysis of large systems. In [31], a Lyapunov function has been developed considering the dynamics of both a conventional generator and a dynamic load. On the same lines it may be possible to develop a nonlinear controller for the VSC in order to take into consideration the dynamics of the load.

This model can be of help in the development of new control techniques and tuning procedures in order to further stabilize systems. Further, the analysis in this paper has been carried out assuming a balanced system condition. The analysis can also be extended to unbalanced systems. An unbalanced system of phasors can be represented as a combination of multiple balanced systems of phasors. This will result in differential equations for each set of balanced phasors. The  $0dq$  transformation for any balanced system of phasors results in a coupled set of equations for the  $d$  and  $q$  axis and an uncoupled equation for the  $0$  axis [26]. As a result, the positive sequence set of phasors and the negative sequence set of phasors give rise to two sets of coupled equations in the  $d$  and  $q$  axis with the difference being in the sign of the speed voltage terms. However, it must be remembered that there are no forcing functions in the negative and zero sequence circuits. The zero sequence currents are known to flow through the neutral terminal to ground. If we assume that all elements, including the inverter, have a neutral to ground connection through a resistance and inductance, the analysis of the zero sequence circuit is akin to the analysis of an uncoupled RL.

## REFERENCES

- [1] P. Zizliauskas, "Subsynchronous torque interaction for HVDC light b-a theoretical description," Master's thesis, Lund Univ., Lund, Sweden, 2001.
- [2] M. Marwali, J.-W. Jung, and A. Keyhani, "Stability analysis of load sharing control for distributed generation systems," *IEEE Trans. Energy Convers.*, vol. 22, no. 3, pp. 737–745, Sep. 2007.
- [3] N. Pogaku, M. Prodanovic, and T. Green, "Modeling, analysis and testing of autonomous operation of an inverter-based microgrid," *IEEE Trans. Power Electron.*, vol. 22, no. 2, pp. 613–625, 2007.

- [4] M. Reza, D. Sudarmadi, F. Viawan, W. Kling, and L. van der Sluis, "Dynamic stability of power systems with power electronic interfaced dg," in Proc. 2006 IEEE PES Power Systems Conf. Expo., 2006 (PSCE'06), 2006, pp. 1423–1428.
- [5] R. Majumder, A. Ghosh, G. Ledwich, and F. Zare, "Stability analysis and control of multiple converter based autonomous microgrid," in Proc. IEEE Int. Conf. Control and Automation, 2009 (ICCA 2009), 2009, pp. 1663–1668.
- [6] D.-J. Lee and L. Wang, "Small-signal stability analysis of an autonomous hybrid renewable energy power generation/energy storage system part I: Time-domain simulations," IEEE Trans. Energy Convers., vol. 23, no. 1, pp. 311–320, Mar. 2008.
- [7] W. Du, H. Wang, X. Zhang, and L. Xiao, "Effect of grid-connected solid oxide fuel cell power generation on power systems small-signal stability," IET Renew. Power Gener., vol. 6, no. 1, pp. 24–37, Jan. 2012.
- [8] D. Gautam, V. Vittal, and T. Harbour, "Impact of increased penetration of DFIG-based wind turbine generators on transient and small signal stability of power systems," IEEE Trans. Power Syst., vol. 24, no. 3, pp. 1426–1434, Aug. 2009.
- [9] J. Slootweg and W. Kling, "The impact of large scale wind power generation on power system oscillations," Elect. Power Syst. Res., vol. 67, no. 1, pp. 9–20, 2003.
- [10] J. Sanchez-Gasca, N. Miller, and W. Price, "A modal analysis of a two-area system with significant wind power penetration," in Proc. IEEE PES Power Systems Conf. Expo., 2004, 2004, vol. 2, pp. 1148–1152.
- [11] T. Knuppel, J. Nielsen, K. Jensen, A. Dixon, and J. Ostergaard, "Small-signal stability of wind power system with full-load converter inter-faced wind turbines," IET Renew. Power Gener., vol. 6, no. 2, pp. 79–91, 2012.
- [12] Y. Mishra, S. Mishra, F. Li, Z.-Y. Dong, and R. Bansal, "Small-signal stability analysis of a DFIG-based wind power system under different modes of operation," IEEE Trans. Energy Convers., vol. 24, no. 4, pp. 972–982, Dec. 2009.
- [13] L. Wang and Y.-H. Lin, "Small-signal stability and transient analysis of an autonomous PV system," in Proc. IEEE/PES Transmission and Distribution Conf. Expo., 2008, 2008, pp. 1–6.
- [14] H. Liu, L. Jin, D. Le, and A. Chowdhury, "Impact of high penetration of solar photovoltaic generation on power system small signal stability," in Proc. Int. Conf. Power System Technology (POWERCON), 2010, 2010, pp. 1–7.
- [15] S. Eftekharnjad, V. Vittal, G. Heydt, B. Keel, and J. Loehr, "Small signal stability assessment of power systems with increased penetration of photovoltaic generation: A case study," IEEE Trans. Sustain. Energy, vol. 4, no. 4, pp. 960–967, 2013.
- [16] B. Tamimi, C. Canizares, and K. Bhattacharya, "Modeling and performance analysis of large solar photovoltaic generation on voltage stability and inter-area oscillations," in Proc. IEEE Power and Energy Society General Meeting, 2011, 2011, pp. 1–6.
- [17] N. Srisaen and A. Sangswang, "Effects of PV grid-connected system location on a distribution system," in Proc. IEEE Asia Pacific Conf. Circuits

and Systems, 2006 (APCCAS 2006), 2006, pp. 852–855.

- [18] C. H. Tie and C. K. Gan, “Impact of grid-connected residential PV systems on the Malaysia low voltage distribution network,” in Proc. IEEE 7th Int. Power Engineering and Optimization Conf. (PEOCO), 2013, 2013, pp. 670–675.
- [19] W. Du, H. Wang, and R. Dunn, “Power system small-signal oscillation stability as affected by large-scale PV penetration,” in Proc. Int. Conf. Sustainable Power Generation and Supply, 2009 (SUPERGEN’09), 2009, pp. 1–6.
- [20] S. Mishra and D. Ramasubramanian, “Phillips-Heffron model for a PV-DG grid connected system,” in Proc. IEEE PES General Meeting, 2013.